Electromagnetic Rotary Tables for Mill and Drill Machining

MARIO STAMANN	THOMAS SCHALLSCHMIDT	ROBERTO LEIDHOLD
Otto von Guericke University	Otto von Guericke University	Otto von Guericke University
Chair of Electrical Drive Systems	Chair of Electrical Drive Systems	Chair of Electrical Drive Systems
Universitätsplatz 2	Universitätsplatz 2	Universitätsplatz 2
39106 Magdeburg	39106 Magdeburg	39106 Magdeburg
GERMANY	GERMANY	GERMANY
mario.stamann@ovgu.de	thomas.schallschmidt@ovgu.de	roberto.leidhold@ovgu.de

Abstract: The following paper shows the control and the practical use of magnetic bearings as rotary tables for mill and drill machining of heavy workpieces. In contrast to conventional rotary tables, magnetic bearings have certain advantages, which can only be used, if a stable and exact position control in five degrees of freedom is implemented. The main focus of this paper is on the cascade control with optimal disturbance rejection, sliding mode control and the decoupling of degrees of freedom.

Key–Words: magnetic bearing, rotary table, degree of freedom, disturbance rejection, cascade control, sliding mode control, decoupling control, multivariable control

1 Introduction

Magnetic bearings are found in a diversity of applications. The most commons are very high speed drives, e.g. [1], and flywheel energy storage systems, e.g. [2]. They can be classified in passive, which are based on superconductors and permanent magnets [3], and active, which are based on electromagnets and a control system [4]. The later ones have the advantage that the characteristics can be adjusted and the position setpoint changed. Rotary tables for machine tools is a less common application for magnetic levitation. It presents particular issues like the high perturbing forces resulting from the milling or drilling operation; elasticity of the moving part due to its form factor and big diameters; low rotating speed; and changing mass and centre of mass due to the different working pieces. Very few contributions regarding magnetic bearings in rotary tables can be found in the literature. Among them, in [5] the design of the magnetic subsystem is addressed for micro-machining.

In the present paper, two rotating tables with different diameters ($1.5 \ m$ and $2 \ m$) and for working pieces of more than one ton, previously introduced in [6], [8], [9], [10], is considered. The aim of this paper is to analyse simple control methods able to initially stabilize the table, even with unknown working pieces and perturbation, in the commissioning process. Once the table is in controlled levitation, identification methods can be applied in order to improve the stiffness, damp oscillations and improve the dynamic. In contrast to conventional bearings, the active

magnetic bearings have the advantages of no mechanical contact between the rotor and the static parts, high damping, nearly infinity static stiffness and adjustable bearing properties (Figure 8). High-precision positioning before and during machining of workpieces, as well as machining on rotating workpieces without changing the mounting position are further benefits of this technology.

On the other hand, the need of additional technical components for active magnetic bearings results in higher costs and more complexness [6].
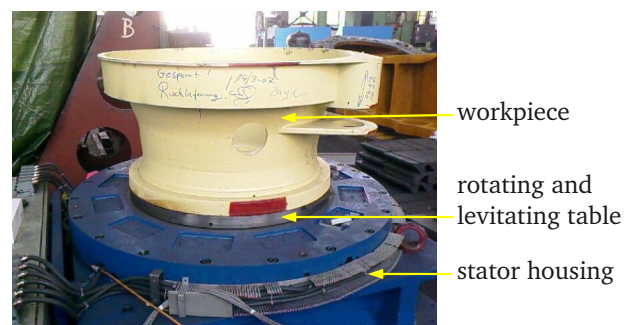
Figure 1: Rotary table prototype 2 (RTP2) with workpiece ($m_w \approx 900 \ kg$)

Figure 1 shows a magnetic bearing as rotary table with a heavy workpiece in a save and stable position. Always attractive magnetic forces are the reason, why the system equilibrium is unstable. Because of very small air gaps under one milimeter and high magnetic forces, high dynamic real-time-control [8] is necessary to stabilise the rotor in five degrees of freedom

by feedback control. Therefore predominantly linear or nonlinear control concepts can be used to control the state vector q in (1), which describes the position and orientation of the rigid rotor in a coordinate system fixed to the stator [9].

$$q = (d_x, d_y, d_z, \phi_x, \phi_y)^T \qquad (1)$$

The sensor and actuator collocation and the rotor position respectively to q are shown in figure 2 examplarily for rotary table prototype 1.
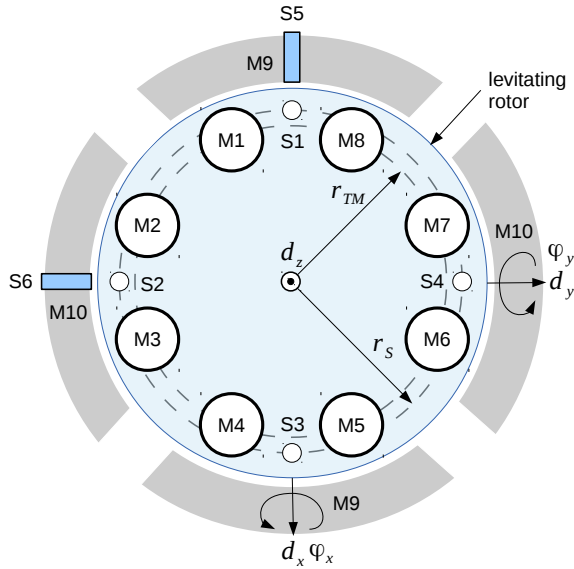
Figure 2: Sensor (S1-S6), supporting actuator (M1-M8) and centering actuator (M9-M10) configuration of rotary table prototype 1

Rotation around z is realised externally by torque motor control unit. For this reason ϕ_z is not part of the rotor position vector q, used for feedback control. To obtain q, a transformation matrix J_{SB} is used to calculate the rotor position depending on the vector of position sensors $x_s = (x_{S1}, ..., x_{S6})^T$ in equation (2).

$$q = J_{SB} \cdot x_s \qquad (2)$$

In the same way a transformation matrix J_{BAF} generates forces $F_A = (F_{M1}, ..., F_{M10})^T$ for each actuator in equation (3), out of forces and moments in relation to a generalised force vector $F_q = (F_x, F_y, F_z, M_x, M_y)^T$ regarding to q [10], [11].

$$F_A = J_{BAF} \cdot F_q \qquad (3)$$

2 Modeling and system identification

For model based control design a plant model with sufficient accuracy in structure and parameters is re-

quired. At first, this can be obtained by considering only one decoupled degree of freedom with later extension to five degrees of freedom, where the coupling can be taken into account.

2.1 Modeling of force actuators

The force generation is realised by hybrid magnets as shown in figure 3. Here the magnetic forces F_o and F_u are produced by the upper and lower hybrid magnet. By superposition of the fields of the permanent magnet and the coil an attractive force is generated. Because of the contrary winding of the upper and lower electromagnet the upper force F_o is strengthened, while the lower force F_u is weakened, when applying a positive current. And vice versa, when a negative current is supplied. Therefore, both positive and negative forces are applicable by defining i_{ref} as reference current, which is applied by current control, using a DC link voltage of $350\ V$ between V_{dd} and V_{ss}. To perform a steady state of the rotor position, the gravity force F_g of the rotorhas to be compensated. This construction is called diffential configuration.
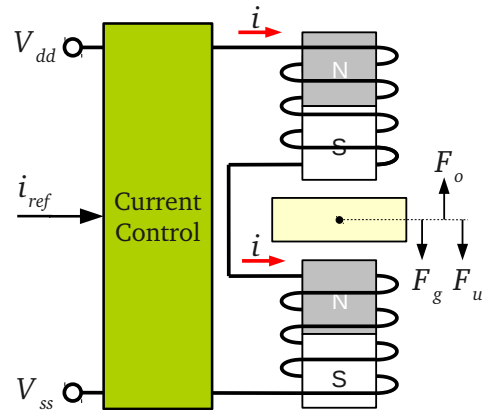
Figure 3: Differential configuration of two hybrid magnets for one degree of freedom

The general magnetic force $F_M(i, d)$ (4) of hybrid magnets is proportional to the square of the current i and the magnetic tension H_0, and inversely proportional to the square of the air gap d [6]. Thereby a is a gain factor containing the number of windings and the geometry.

$$F_M(i, d) = a \cdot \frac{(i + H_0)^2}{d^2} \qquad (4)$$

Superposition of upper and lower magnetic forces in differential configuration leads to $F_{M,hyb}(i, d_o, d_u)$ with the air gaps d_o and d_u (5).

$$F_{M,hyb}(i, d_o, d_u) = F_o(i, d_o) - F_u(-i, d_u) \qquad (5)$$

Defining d in (6) as the position of the rotor within the full air gap distance d_{max}, d_o is determined with the equation (7).

$$
\begin{aligned}
d &= d_u & (6)\\
d_o &= d_{max} - d & (7)
\end{aligned}
$$

Equation (8) describes the magnetic force $F_{M,hyb}(i,d)$ using (4), (5), (6) and (7). Because of safety bearings, the minimum air gap is d_{min}. For simplification $k_1 = k_2 + d_{max}$ and $k_2 = d_{min}$ are used in (8). The identification problem is to find the four parameters k_1, k_2, a and H_0 to describe the nonlinear algebraic characteristic curve (8). For this, an already stable control configuration or an external force measuring test environment is needed to identify the set of parameters.

$$
F_{M,hyb} = a \left[\frac{(i+H_0)^2}{(k_1-d)^2} - \frac{(-i+H_0)^2}{(k_2+d)^2} \right] \quad (8)
$$

The current for each pair of hybrid magnets is supplied via a separate current controller, which causes a dynamic transient behaviour. Figure 4 shows the measured step responses for a set point current of 2 A for the supporting and the centering hybrid magnet pair. Because of different mechanical construction, there are differences in dynamics between centering and supporting actuators.
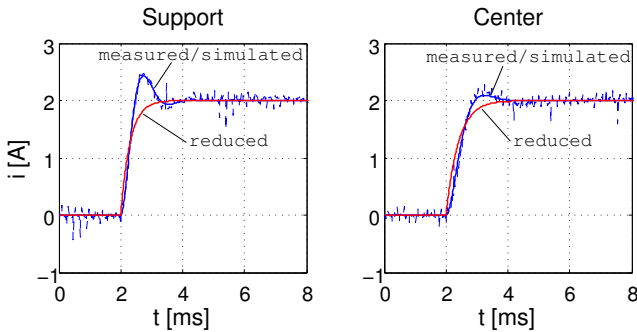
Figure 4: Measured, simulated and reduced model step responses for a set point current of 2 A (Prototyp 1), supporting pair of hybrid magnets (left) and centering pair of hybrid magnets (right)

The dynamic transient behaviour of one current control loop with i_{ref} as reference current and i as current through the winding, can be described by a second order continous transfer function (9) based on optimum amount [7] with the fundamental time constant T_f.

$$
G_c(s) = \frac{i(s)}{i_{ref}(s)} = \frac{1}{1 + 2T_f s + 2T_f^2 s^2} \quad (9)
$$

In terms of system order reduction and because of the very small time constant of $T_f = 0.22\ ms$, which was determined by using the method of least squares, it is possible to neglect the quadratic term $2T_f^2 s^2$, so we get (10) with $T_i = 2T_f$.

$$
G_c(s) = \frac{i(s)}{i_{ref}(s)} = \frac{1}{1 + T_i s} \quad (10)
$$

Figure 4 shows measured and simulated current step responses by (9) and the approximated behaviour of the current control loop by order reduction (10). It can be seen, that the order reduction describes the transient behaviour without overshoot. This neglect is used for control design and has no significant effect on the control behaviour.

2.2 Plant model for one degree of freedom

Under assumption of a rigid rotor body the following block diagram (Figure 5) reflects the nonlinear dynamic plant behaviour in one degree of freedom. Thereby $F_{M,hyb}$ is the nonlinear force characteristic (8), d is the measureable position as plant output and i_{ref} the plant input. The acceleration due to gravity g is only acting as constant disturbing force in oposite direction d_z.
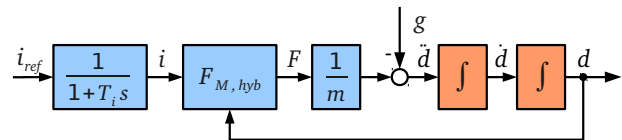
Figure 5: Block diagram of the nonlinear magnetic bearing plant in one degree of freedom

By definition of the state variables x_1, x_2 and x_3 (11), the overall system equations can be written as follows in (12) with input $u = i_{ref}$.

$$
(x_1, x_2, x_3)^T = (d, \dot{d}, i)^T \quad (11)
$$

$$
\begin{pmatrix} \dot{x}_1 \\ \dot{x}_2 \\ \dot{x}_3 \end{pmatrix} = \begin{pmatrix} x_2 \\ \frac{1}{m} F_{M,hyb}(x_3, x_1) - g \\ -\frac{1}{T_i} x_3 + u \end{pmatrix} \quad (12)
$$

A linear state space model can be derived by linearisation of the force characteristic $F_{M,hyb} =$

$f(x_3, x_1)$ for one point of operation $\boldsymbol{x}^b = (x_1^b, 0, x_3^b)^T$ along the dependent variables x_3 (13) and x_1 (14).

$$k_i = \left.\frac{\partial F_{M,hyb}(x_3, x_1)}{\partial x_3}\right|_{x_3 = x_3^b} \tag{13}$$

$$k_s = \left.\frac{\partial F_{M,hyb}(x_3, x_1)}{\partial x_1}\right|_{x_1 = x_1^b} \tag{14}$$

The obtained linear force parameters k_i and k_s, following the linear state space model (15), in point of operation, can be used for the linear control design. The state space vector $\boldsymbol{x}$ conforms to the variation around $\boldsymbol{x}^b$.

$$\dot{\boldsymbol{x}} = \begin{pmatrix} 0 & 1 & 0 \\ \frac{k_s}{m} & 0 & \frac{k_i}{m} \\ 0 & 0 & -\frac{1}{T_i} \end{pmatrix} \boldsymbol{x} + \begin{pmatrix} 0 \\ 0 \\ 1 \end{pmatrix} u$$

$$y = \begin{bmatrix} 1 & 0 & 0 \end{bmatrix}^T \boldsymbol{x} \tag{15}$$

Getting these parameters by experimental system identification is only possible in a stable system configuration. For first commissioning of magnetic bearings, robust control implementation can be applied by using a sliding mode controller with limited reference current as controller output.

Table 1: Operation point parameters for rotary table prototype 1 (RTP1) in the supporting degree of freedom (z-axis)

m	k_i	k_s	T_i
$1867\ kg$	$530\ \frac{N}{A}$	$110.6 \cdot 10^6\ \frac{N}{m}$	$0.44 \cdot 10^{-3}\ s$

Table 1 shows for example the linear plant parameters of the rotary table prototyp 1. These set of parameters were found by experimental system identification for one point of operation $x_1^b = 0.595\ mm$ and $x_3^b = 0\ A$ in d_z direction. Because of the very small time constant T_i in comparison with the sample time $T_S = 0.5\ ms$ of the real-time-processing, it is possible to neglect the dynamic behaviour to get a simplified state space model (16) for control design. This simplification can later be taken into account by a summarised time constant T_Σ.

$$\dot{\boldsymbol{x}} = \begin{pmatrix} 0 & 1 \\ \frac{k_s}{m} & 0 \end{pmatrix} \boldsymbol{x} + \begin{pmatrix} 0 \\ \frac{k_i}{m} \end{pmatrix} u$$

$$y = \begin{bmatrix} 1 & 0 \end{bmatrix}^T \boldsymbol{x} \tag{16}$$

The new system input $u = i = i_{ref}$ can be interpreted as a magnetic force, while the output y is the measured position of the corresponding degree of freedom.

2.3 Plant model for five degrees of freedom

For five degrees of freedom the following linear state space model (17) with the mass matrix $\boldsymbol{M}$ and the diagonal matrices $\boldsymbol{k}_i$ and $\boldsymbol{k}_s$ can be derived from (16).

$$\dot{\boldsymbol{x}} = \begin{pmatrix} 0 & \boldsymbol{I} \\ \boldsymbol{I}\boldsymbol{M}^{-1}\boldsymbol{k}_s^T & 0 \end{pmatrix} \boldsymbol{x} + \begin{pmatrix} 0 \\ \boldsymbol{I}\boldsymbol{M}^{-1}\boldsymbol{k}_i^T \end{pmatrix} \boldsymbol{u}$$

$$\boldsymbol{y} = \begin{pmatrix} \boldsymbol{I} & 0 \end{pmatrix} \boldsymbol{x} \tag{17}$$

The system input vector $\boldsymbol{u}$ consists now of five magnet currents respectively to each degree of freedom, while the output $\boldsymbol{y}$ is the measured position of the rigid rotor and therefore equivalent to the state vector $\boldsymbol{q}$ (1).

$$\boldsymbol{M} = \begin{pmatrix} m & . & . & . & 0 \\ . & m & & & . \\ . & & m & & . \\ . & & & J_x & . \\ 0 & . & . & . & J_y \end{pmatrix} \tag{18}$$

Assuming a diagonal mass matrix $\boldsymbol{M}$ of the plant model, a completely decoupled feedback control of each degree of freedom is possible. The mass parameter m and the moments of inertia J_x and J_y can be fairly precisely quantified by CAD tool simulation.

3 Feedback control design

3.1 Cascade control

For practical points of view it was determined, that cascade control is an advantageous control concept, especially for first time implementing and for control under real conditions. This concept makes it possible to separately adjust the dynamic stiffness and damping of the levitating rotor by a suitable choice of the controller parameters. In addition, limitations of the physical state variables current, velocity and position can be easily integrated, with the possibility of pre-steering all state variables, in case of using a trajectory generator [11].

Figure 6 shows the control structure of the cascade control. The inner velocity closed loop can be designed as a first order transfer element, by compensating the magnetic force in dependence of the air gap.

This can be achieved by direct feedforward control of the measured displacement d and closing the inner loop through the velocity controller P_{qq}.
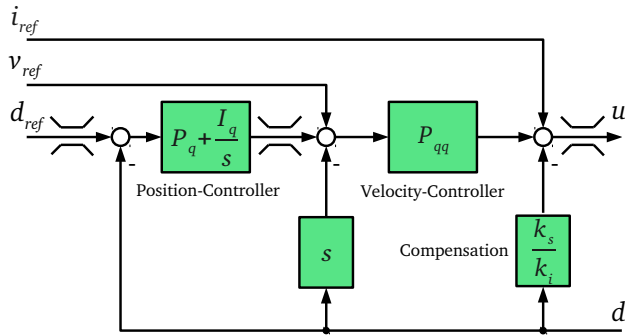
Figure 6: Block diagram of the cascade controller for one degree of freedom with additional pre-steering inputs i_{ref} and v_{ref}

$$P_{qq} = \frac{m}{T_\Sigma k_i} \qquad (19)$$

Under assumption, that the parameters m and k_i are fairly precisely known, with P_{qq} in (19) the inner closed loop gets approximately first order transfer behaviour with the time constant T_Σ. All small time constants are included in T_Σ as a sum. For optimal disturbance rejection the parameters P_q and I_q for the outer PI controller (symmetrical optimum) have to adjust like (20), to get a symmetrical open loop amplitude frequency response (Figure 7) around the pass through frequency $\omega_D = (2T_\Sigma)^{-1}$ [7].
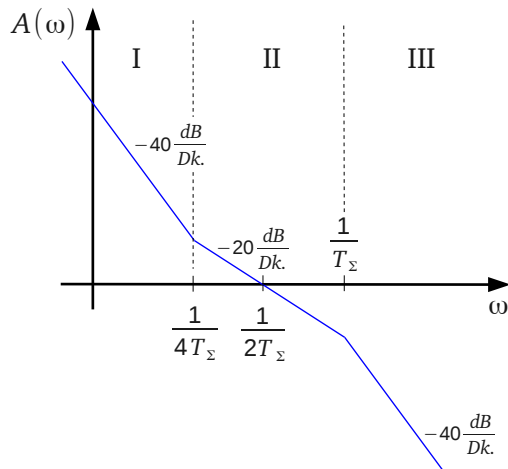
Figure 7: Symmetrical open loop shaping around $\omega_D = (2T_\Sigma)^{-1}$ for optimal disturbance rejection with a maximum of phase reserve

$$P_q = \frac{1}{2T_\Sigma} \qquad I_q = \frac{1}{8T_\Sigma^2} \qquad (20)$$

Thereby the adjustment of T_Σ defines the dynamic stiffness of the levitating rotor, related to the stator housing. High values of T_Σ result in softer bearing properties, but because of sinking damping also in higher risk of instability. On the other hand, smaller values of T_Σ give more stiffness, but increase high frequency signal components. In both cases there always have to be enough phase reserve for a stable loop. This implies, that T_Σ can be adjusted only in a restricted range. Taking into account, that the discrete controller realisation adds additional delay into the open control loop, due to the sample time $T_S = 0.5~ms$, and that additional signal filtering with $T_F = 1~ms$ is necessary, the minimal value of T_Σ for stable loop can not be smaller than $T_i + T_F + T_S \geq 2~ms$.

$$G_c(s) = \frac{d(s)}{d_{ref}(s)} = \frac{1}{1 + 4T_\Sigma s + 8T_\Sigma^2 s^2 + 8T_\Sigma^3 s^3} \qquad (21)$$

$$G_d(s) = \frac{d(s)}{F_d(s)} = \frac{8T_\Sigma^3}{m} \frac{s}{1 + 4T_\Sigma s + 8T_\Sigma^2 s^2 + 8T_\Sigma^3 s^3} \qquad (22)$$

The ideal closed loop control behaviour can be described by the transfer function $G_c(s)$ (21), while the ideal disturbance behaviour is characterised by $G_d(s)$ (22).
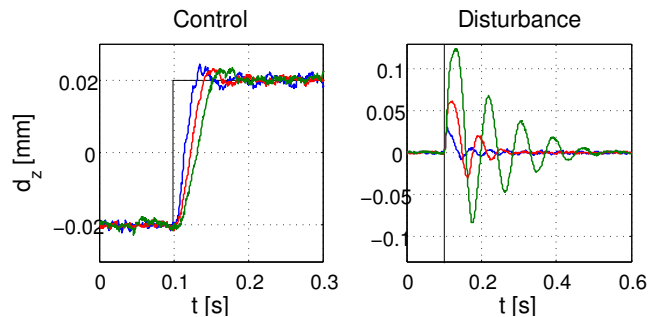
Figure 8: Control and disturbance step responses by changing the controller parameter $T_\Sigma = 4~ms$, $T_\Sigma = 6~ms$ and $T_\Sigma = 8~ms$ on RTP1 (experimental)

As can be seen in Figure 8, the variation of T_Σ influences the dynamic of the control behaviour and the dynamic bearing stiffness. Because of unmodeled dynamics in the control loop and digital implementation with fixed sampling rate, the bearing damping also varies with T_Σ. However by defining of only one controller parameter, it is possible to influence the dynamic behaviour respectively the bearing stiffness, while symmetrical optimised control performance is ensured.

Figure 9 shows step responses of cascade control configuration with $T_\Sigma = 5~ms$ for different mass
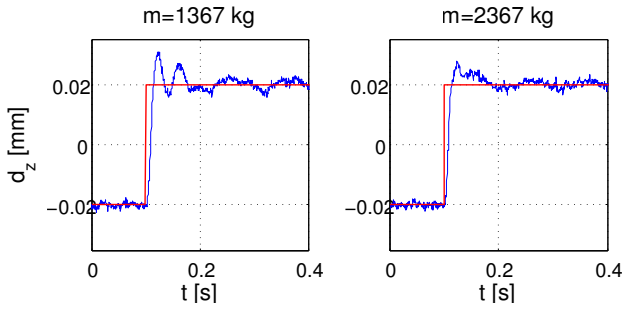
Figure 9: Non pre-filtered step responses by cascade control for a setpoint step of $\Delta d_{ref} = 40\ \mu m$ and different overall rotor masses ($T_\Sigma = 5\ ms$ - RTP1) (experimental)

loads. As can be seen, if the mass is varying in a wide range, the step responses show different dynamical response behaviour. Even unstable system responses are expected in case of larger variations, which cannot be quantified, because unstable operation for this real application is not desired. Measured disturbance responses with a force step of $F_d = 2\ kN$ are visible in figure 10, where the disturbance displacement depends on the rotor mass.
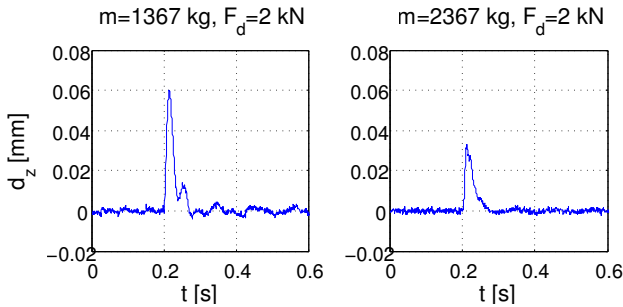
Figure 10: Disturbance responses by cascade control for a setpoint step of $F_d = 2\ kN$ with different overall rotor masses ($T_\Sigma = 5\ ms$ - RTP1) (experimental)

Looking at the disturbance transfer function for symmetrical optimized magnetic bearings (22), exhibits that the dynamic stiffness depends on the values of m and T_Σ. Larger masses and a smaller T_Σ lead to a better dynamic bearing stiffness. As can be seen, with an additional load of $1000\ kg$ the dynamic stiffness is almost twice as high as without load. For this reason mass adaptation and robust control methods are desired.

3.2   Sliding mode control

The main advantage of sliding mode control is its robustness against variations of plant parameters and external disturbances. In fact, that the controller is

switching between two different control laws dependent on the state vector, sliding modes occur. For linear systems (23) the control law is defined by (24) with the switching function (25).

$$\dot{\boldsymbol{x}} = \boldsymbol{A}\boldsymbol{x} + \boldsymbol{b}u \tag{23}$$

$$u(\boldsymbol{x}) = \begin{cases} +u_{max} & \text{for} \quad s_w(\boldsymbol{x}) > 0 \\ -u_{max} & \text{for} \quad s_w(\boldsymbol{x}) < 0 \end{cases} \tag{24}$$

$$s_w(\boldsymbol{x}) = \boldsymbol{k}^{\boldsymbol{T}}\boldsymbol{x} \tag{25}$$

To guarantee that all system trajectories at state space reach the switching area $s_w(\boldsymbol{x})$ in finite time, the conditions (26) and (27) by Gao and Hung [13] have to comply.

$$s_w(\boldsymbol{x})\dot{s}_w(\boldsymbol{x}) < 0 \tag{26}$$

$$\dot{s}_w(\boldsymbol{x}) = u_{max} \cdot sgn(s_w(\boldsymbol{x})) - d \cdot s_w(\boldsymbol{x}) \tag{27}$$

Out of these conditions the following control law (28) can be derived for one degree of freedom.

$$u(\boldsymbol{x}) = -\frac{\boldsymbol{k}^T \boldsymbol{A}\boldsymbol{x} + u_{max} \cdot sgn(\boldsymbol{k}^T \boldsymbol{x}) + d \cdot \boldsymbol{k}^T \boldsymbol{x}}{\boldsymbol{k}^T \boldsymbol{b}} \tag{28}$$

Adjusting the dynamic behaviour of the control loop is possible by setting the parameters u_{max}, d and $\boldsymbol{k}$. For the linear state space model (16) an additional integral state feedback is necessary for sliding mode control to get stationary accuracy. Therefore (29) is the basic model for sliding mode control design with the new state x_1, when $\dot{x}_1 = x_2$, $x_2 = d$ and $x_3 = \dot{d}$.

$$\dot{\boldsymbol{x}} = \begin{pmatrix} 0 & 1 & 0 \\ 0 & 0 & 1 \\ 0 & \frac{k_s}{m} & 0 \end{pmatrix} \boldsymbol{x} + \begin{pmatrix} 0 \\ 0 \\ \frac{k_i}{m} \end{pmatrix} u$$

$$y = \begin{bmatrix} 0 & 1 & 0 \end{bmatrix}^T \boldsymbol{x} \tag{29}$$

The switching parameter vector $\boldsymbol{k}^T$ of the switching function $s_w(\mathbf{x})$, can be determined as a state feedback from the cascade control parameters (30).

$$\boldsymbol{k}^T = \frac{m}{k_i} \left(\frac{1}{8T_\Sigma^3,} \quad \frac{1}{2T_\Sigma^2,} \quad \frac{1}{T_\Sigma} \right) \tag{30}$$

By choosing $d = 0$ and $T_\Sigma = 5\ ms$ the step responses in sliding mode configuration for one degree of freedom are shown in figure 11.

In spite of mass parameter variations of $1000\ kg$, the closed loop dynamic behaviour is completely unaffected in contrast to the before investigated cascade
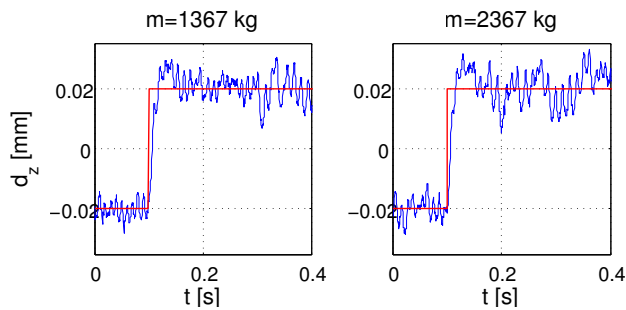
Figure 11: Step responses by sliding mode control for a setpoint step of $\Delta d_{ref} = 40\ \mu m$ and different overall rotor masses ($T_\Sigma = 5\ ms$ - RTP1) (experimental)
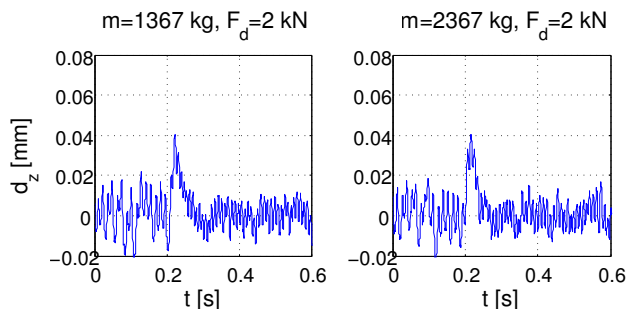
Figure 12: Disturbance responses by sliding mode control for a force step of $F_d = 2\ kN$ and different overall rotor masses ($T_\Sigma = 5\ ms$ - RTP1) (experimental)

control concept. The investigation of external disturbance force rejection also yields robust dynamic stiffness for different mass loads (Figure 12).

Because of the actuator dynamics and discret control implementation, highfrequently switching occurs by using sliding mode control. Therefore the position accuracy and the accoustic noise in steady state is worse than in cascade control. This so called chattering and is visible by comparison of the noise intensity between figures 9-10 and figures 11-12. The chattering problem can be decreased by using different methods improving the control law [12].

In case of commissioning magnetic bearings with unprecisely known system parameters, sliding mode control is a promising option to first get a stable rotor position in all degrees of freedom. Because of limiting the actuator force by the control law, mechanical stress can be reduced in case of unstable operation. This is very important especially for big rotary tables. On this basis, identification methods can be applied to get nearly exact system parameters.

3.3 Decoupling control

Disturbance forces during machining of workpieces on an electromagnetic rotary table cause periodic displacements of the rotor position. A milling process of a heavy workpiece on rotary table prototyp 2 is shown in figure 13.

Figure 13: Workpiece milling on rotary table prototype 2 (RTP2) ($m_w \approx 1900\ kg$)

Machining forces are acting in different space directions, so that position displacements also appear in different controlled degrees of freedom with various amplitudes and frequencies. For a drilling process, using a drill with a diameter of $30\ mm$, the displacement d_y over time is plotted in figure 14.

As can be seen in figure 14 left, vibrations appear during the drill process. The controller is able to compensate stationary disturbance forces completely by current adaptation, visible in figure 14 right. Only dynamic force components lead to vibrations at a fundamental frequency of about $8\ Hz$, which cannot be completely compensated, because of the limited dynamic bearing stiffness (22) by the cascade controller.
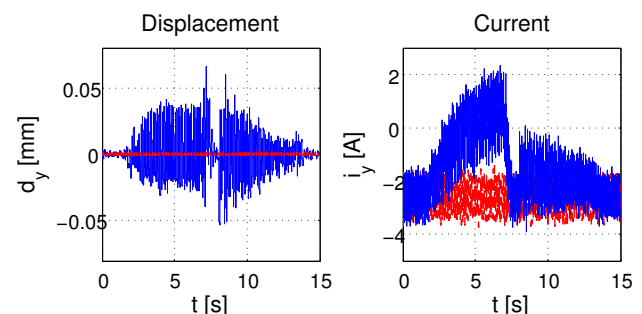
Figure 14: Displacement d_y and current i_y over time during workpiece drilling, using a $30\ mm$ drill ($T_\Sigma = 12\ ms$ - RTP2) (experimental)

Matrix frequency response investigations (Figure 15) have figured out, that there are significantly couplings between the degrees of freedom, even if the plant is transformed into a decoupled control structure. The main reason for this is the center of gravity of the levitating rotor, which is not exactly located at

the reference point of the transformation. Since different workpieces are rigidly connected to the levitation rotor, displacements of the center of gravity are expected. Furthermore flux leakage of the magnetic actuators also can lead to not desired coupling forces and moments.
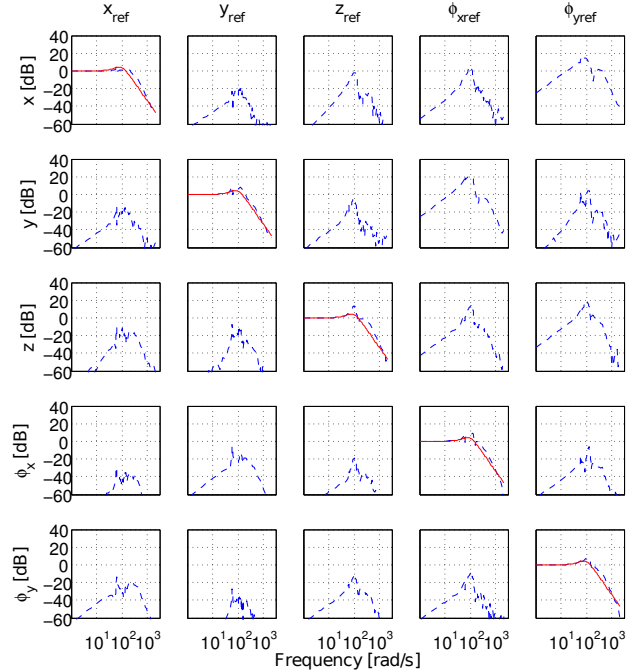
Figure 15: Measured matrix frequency response (dashed) in comparison with simulated decoupled control behaviour ($T_\Sigma = 5\ ms$ - RTP1) (experimental)

These couplings are visible in the non-diagonal frequency responses in figure 15 and look similar to commonly disturbance frequency responses. This seems to be clear, because the controller is optimised to eleminate disturbance forces. The diagonal frequency responses of figure 15 show the measured control behaviour for each degree of freedom, compared to the desired ones described by (21). It is strikingly, that there are resonances, which are apparently caused by the couplings.

To take these couplings into account in the plant model, a space vector $\boldsymbol{r}_{BC}$ (31) is used to describe the distance from the center of gravity (C) to the reference point of the coordinate transformation (B). This is illustrated in figure 16. The forces F and moments M are acting on the reference point.

$$\boldsymbol{r}_{BC} = (r_{d_x}, r_{d_y}, r_{d_z})^T \qquad (31)$$

When r_{d_x}, r_{d_y} and r_{d_z} are not zero, the diagonal mass matrix $\boldsymbol{M}$ in (18) gets non-diagonal first order moments (32). For the symmetrical rotor J_x is identical to J_y while couplings can be described by the moment of deviation J_{xy} as non-diagonal elements of the intertia tensor. The mass matrix now consists of a (3x3) diagonal matrix for the translational degrees of freedom, of the (2x2) inertia tensor and of the first order moments arranged in mirror symmetry [6],[14].
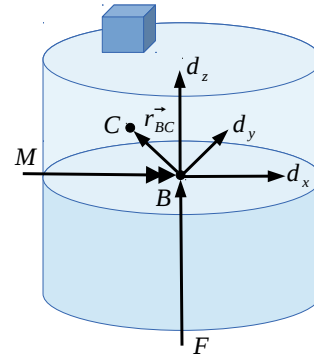
Figure 16: Space vector $\boldsymbol{r}_{BC}$ describing the distance between center of gravity (C) and reference point (B) of the levitating rotor

$$\mathbf{M} = \begin{pmatrix} m & 0 & 0 & 0 & mr_{d_z} \\ 0 & m & 0 & -mr_{d_z} & 0 \\ 0 & 0 & m & mr_{d_y} & -mr_{d_x} \\ 0 & -mr_{d_z} & mr_{d_y} & J_x & J_{xy} \\ mr_{d_z} & 0 & -mr_{d_x} & J_{xy} & J_y \end{pmatrix} \qquad (32)$$

Assuming the parameters of table 2 the model behaviour in comparison to the experimental frequency plots can be seen in figure 17. Because of model parameter uncertainties, signal filtering and magnetic leakage flux, the modeling of couplings can only be achieved approximately.

Table 2: Coupling parameters for RTP1 without workpiece

r_x	r_y	r_z	J_{xy}
$-0.05\ m$	$-0.05\ m$	$0.027\ m$	$36\ kg \cdot m^2$

The resonances already mentioned in relation to figure 15 now also appear in the plant model (Figure 17).

Vibrations by machining caused in one degree of freedom, can easy propagate into other degrees of freedom, if the control system is not completely decoupled. Therefore first decoupling of the plant is necessary and then vibration damping methods can be applied. Using the inverse $\boldsymbol{M}^{-1}$ of the non-diagonal mass matrix (32) for designing the velocity controller
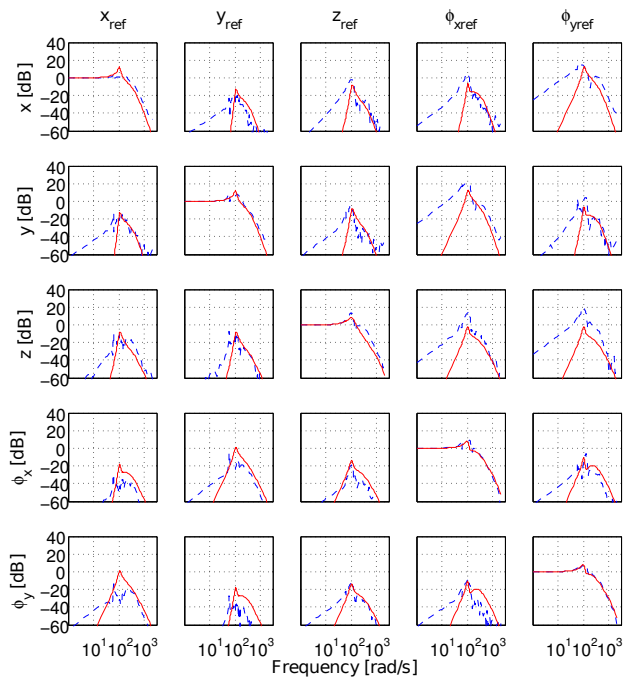
Figure 17: Simulated coupled control behaviour in comparison to the measured matrix frequency response (dashed). ($T_\Sigma = 5\ ms$ - RTP1) (experimental)

in figure 6, all couplings can be compensated in addition to the mass compensation.
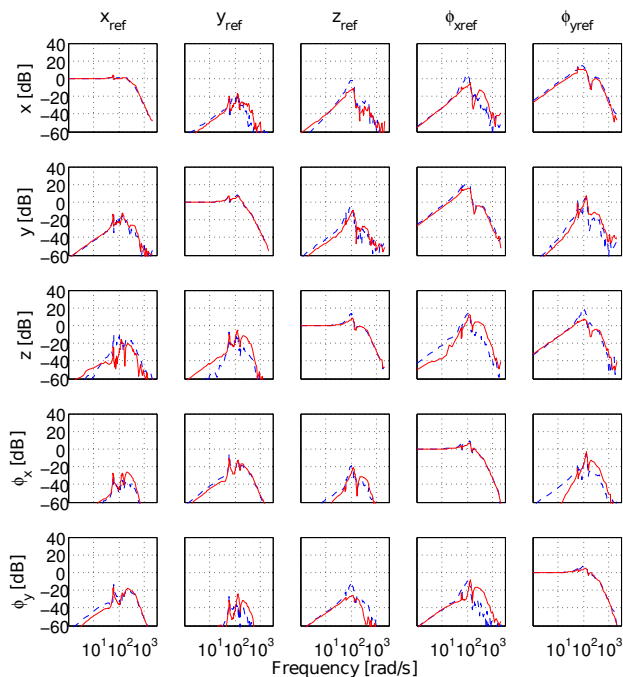
Figure 18: Matrix frequency response for the decoupled feedback control in comparison to figure 15 (dashed). ($T_\Sigma = 5\ ms$ - RTP1) (experimental)

The measured frequency response plotted in figure 18 shows the control behaviour of the decoupled system using the parameters in table 2. Because of time delay by the current controllers and not exactly known parameters, decoupling is only approximately reachable. However, in some frequency responses the maximum coupling amplitude could be decreased by more than 10 dB.

4   Conclusion

This paper has presented the control design for magnetic bearings as rotary table for mill and drill machining of large and heavy workpieces. Model based cascade control and sliding mode control concepts for optimal disturbance rejection in five degrees of freedom has been shown. The investigation of couplings in the control structure has figured out, that first decoupling is necessary to improve the control performance and establish a basis for vibration damping of milling and drilling processes on the table. Further research needs to be done for online and offline identification of the mass matrix and for decoupling of external disturbance forces by drill and mill machining.

References:

[1] C.-R. Sabirin and A. Binder, *Rotor levitation by active magnetic bearing using digital state controller,* in EPE-PEMC, 2008, pp. 1625-1632.

[2] M. Subkhan and M. Komori, *New Concept for Flywheel Energy Storage System Using SMB and PMB,* IEEE Transactions on Applied Superconductivity, vol. 21, 2011, pp. 1485-1488.

[3] S.-O. Siems and W.-R. Canders, *Advances in the design of superconducting magnetic bearings for static and dynamic applications,* Superconductor Science and Technology, 2005, p. S86.

[4] T. Schuhmann, W. Hofmann and R. Werner, *Improving Operational Performance of Active Magnetic Bearings Using Kalman Filter and State Feedback Control,* Industrial Electronics, IEEE Transactions on, vol. 59, 2012, pp. 821-829.

[5] R. Banucu, J. Albert, V. Reinauer, C. Scheiblich, W.-M. Rucker, A. Hafla and A. Huf, *Automated*

Optimization in the Design Process of a Magnetically Levitated Table for Machine Tool Applications, IEEE Transactions on Magnetics, vol. 46, 2010, pp. 2787-2790.

[6] O. Petzold, *Modellbildung und Untersuchung eines magnetisch gelagerten Rundtisches,* Dissertation Otto von Guericke University Magdeburg, 2006.

[7] D. Schröder, *Elektrische Antriebe 2, Regelung von Antrieben,* Springer Verlag Berlin Heidelberg, 1995

[8] S. Palis, M. Stamann and T. Schallschmidt, *Rechnergestützter Reglerentwurf für ein Magnetlager mit Scilab/Scicos-RTAI,* EKA Mageburg, 2008.

[9] M. Stamann, T. Schallschmidt and F. Palis, *Aktive Schwingungsdämpfung unter Berücksichtigung der Nichtlinearitäten am Beispiel magnetisch gelagerter Maschinenrundtische,* 10. Magdeburger Maschinenbau Fachtagung, 2011.

[10] S. Palis, M. Stamann and T. Schallschmidt, *Nonlinear adaptive control of magnetic bearings,* EPE Aalborg, 2007.

[11] T. Schallschmidt, *Modellbasierte Regelung magnetisch gelagerter Rundtische,* Dissertation Otto von Guericke University Magdeburg, 2012.

[12] V. Utkin, J. Guldner and J. Shi, *Sliding Mode Control in Electro-Mechanical Systems,* CRC Press by Taylor & Francis Group, 2009.

[13] W. Gao and J.-C. Hung, *Variable Structure Control of Nonlinear Systems: A New Approach.,* IEEE Transactions on Industrial Electronics, 1993.

[14] M. Ruskowski, *Aufbau und Regelung aktiver Magnetführungen,* Dissertation University Hannover, 2004.